Elastic and Inelastic Scattering of E/A=13 MeV ^{24}Mg on ^{12}C

R. Alfaro-Molina*, M.E. Brandan*, A. Menchaca Rocha*, S. Gallardo*, K. Hagel, N. Marie,
J.B. Natowitz, R. Wada, and Y. Zhao
**Instituto de Física UNAM Mexico City, Mexico.*

Recent ^{12}C+^{24}Mg elastic scattering measurements at energies near the Coulomb barrier [1] indicate that nuclear refraction effects may still be present in this heavy system, therefore, the discrete ambiguities found at lower energies (2 MeV/amu) can be understood and eliminated if data at higher energies (>10 Mev/amu) are available [2].

The experiment was performed in the scattering chamber of the SEE Line which allowed us to set and move detectors with the position resolution required for this kind of measurement. The beam of ^{24}Mg particles from the Texas A&M K500 superconducting cyclotron bombarded a 100 μgr/cm^2 ^{12}C target on which a thin layer (4.5 μg/cm^2) of ^{197}Au was evaporated. The ^{24}Mg scattered ions were detected using a small one-dimensional multiwire proportional chamber (MWCP) and two multi-strip solid state counters. One of them acted as the E detector in a telescope array with the MWPC [3], while the second multi-strip counter was used to detect the recoiling ^{12}C ions (the ^{197}Au ions were stopped inside the target).

The angular region covered was from θ_{lab}=3 to θ_{lab}=21 degrees (corresponding θ_{cm}=8, θ_{cm}=55) with an angular resolution of θ_{cm}=0.3 degree. The energy resolution (600 KeV at small angles) was sufficient to separate the ^{24}Mg elastic and the first excited state (Ex=1.37) however, as we advanced toward larger angles (θ_{cm} >35 degrees), due to the large kinematic dependence it was not possible to separate them clearly.

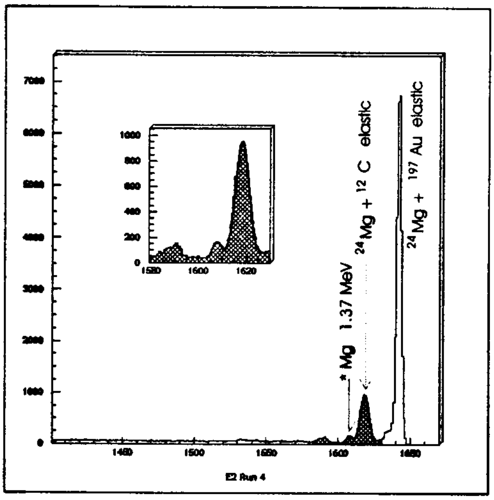

Fig. 1 Sample espectrum at θ_{lab}= 7°.

The elastic and inelastic scattering angular distributions were determined by direct peak integration or by gaussian fitting when the peaks were not well resolved (fig.1). The absolute normalization was obtained from elastic scattering of ^{24}Mg by the ^{197}Au layer, which at these angles is dominated by Rutherford scatteringAn optical model analysis (OM) was performed, assuming phenomenological potentials with Wood-Saxon shapes for the real and imaginary parts. The optimization of the six parameters was done using the code PTOLEMY [4], starting from initial parameters which covered a wide range of values, 55<V_0<400 MeV and 16<W_0<36 MeV. From this analysis it was found that a good fit can be achieved using a potential whose imaginary part is weakly absorbing while for some of them, the real part is deep enough to sustain a nuclear rainbow (fig 2). The parameters of the different optical potentials are summarized in Table I.

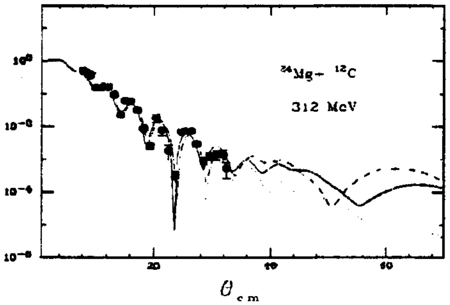

Fig 2. Measured diferential elastic cross section and optical-model calculations by potential in Table I.

Furthermore, the real and imaginary parts follow the V/W systematics found in that system on which refractive effects have been observed [5]. An analysis using the NEAR-FAR decomposition technique, shows that nuclear refraction is present however, it starts to be dominant, at least, at $\theta_{cm}=40^0$, so its effect can not be clearly observed in the angular distribution (fig.3). In order to better restrict the potential shape a coupled channel analysis was carried out. In this case the free parameters were the deformation length, and the imaginary potential depth.

The initial potentials used were those found in the OM analysis. The real part was preserved while the imaginary was modified allowing a variation of 15% in their deepness.

The result from this analysis is that a reduction of 10% in the deepness and a deformation length within a range of 1.38 to 1.5 fm (which agrees with values reported in the literature) can fit the data fig (4). Therefore it is not possible to restrict the potential shape from this result.

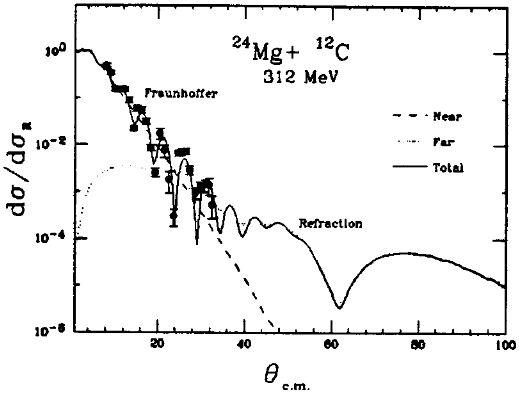

Fig 3. Near-Far decomposition of the cross-section calculation. After 40° the Far side contribution is dominant.

In summary, evidence of nuclear refraction has been observed in this system via the V/W systematics and the near-far decomposition of the scattering amplitude obtained from potentials that fit the data. The ambiguities in the potential characteristics that still persist might be resolved by more complete measurements at this, or higher energies.

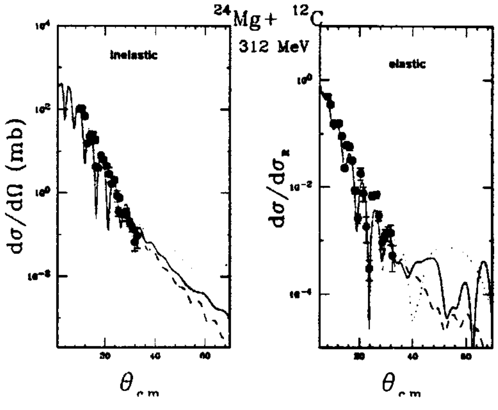

Fig 4. Measured differential cross section and CC calculations for elastic and inelastic scattering.

Table I. The parameters of Wood-Saxon optical potentials obtained from the OM analysis.

V MeV	**R** fm	**a** fm	**W** MeV	**R_i** fm	**a_i** fm
180	3.52	0.88	16.0	5.94	0.88
280	3.21	0.88	24.0	5.49	0,78
340	3.05	0.88	28.0	5.38	0.79

References

[1] W. Sciani, A. Lépine-Szily, R. Litchtenthaler, F.P Fachini, L.C. Gomes, G.F. Lima, M.M. Obuti, J.M. Oliveira Jr., Nuc. Phys. A **620**, 91 (1997).

[2] M.E. Brandan and G.R. Satchler, Phys. Rep. **285**, 143 (1997).

[3] R. Alfaro-Molina, A. Martinez-Davalos, A. Menchaca-Rocha, K. Hagel, J.B. Natowitz, R. Wada, Y. Zhao, Nuc. Inst. Meth. A **392**, 447 (1997).

[4] M.H. Macfarlane and S.C. Pieper, Argonne Nat. Lab. Rep. No. ANL-76-11, Rev. 1 (1978).

[5] M.E. Brandan and K. McVoy, Phys. Rev. **C** **53**, 1362 (1997).